KAPL-P-000055
(K96074)

CONF-9606116--

EFFECT OF IRRADIATION ON THERMAL EXPANSION OF SICF/SIC COMPOSITES

D.J. Senor, D.J. Trimble, J.J. Woods

June, 1996

NOTICE

KAPL ATOMIC POWER LABORATORY SCHENECTADY, NEW YORK 12301

Operated for the U. S. Department of Energy
by KAPL, Inc. a Lockheed Martin company

MASTER

DISCLAIMER

DISCLAIMER

Portions of this document may be illegible in electronic image products. Images are produced from the best available original document.

Effect of Irradiation on Thermal Expansion of SiC_f/SiC Composites

D.J. Senor[1], D.J. Trimble[2], and J.J. Woods[3]

[1]Pacific Northwest Laboratory*, Richland, WA, 99352
[2]Westinghouse Hanford Company, Richland, WA 99352
[3]Lockheed Martin, Schenectady, NY 12301

*Operated for the U.S. Department of Energy by Battelle Memorial Institute under contract DE-AC06-76RLO 1830.

ABSTRACT

Linear thermal expansion was measured on five different SiC-fiber-reinforced/SiC-matrix (SiC_f/SiC) composite types in the unirradiated and irradiated conditions. Two matrices were studied in combination with Nicalon CG reinforcement and a 150 nm PyC fiber/matrix interface: chemical vapor infiltrated (CVI) SiC and liquid-phase polymer impregnated precursor (PIP) SiC. Composites of PIP SiC with Tyranno and HPZ fiber reinforcement and a 150 nm PyC interface were also tested, as were PIP SiC composites with Nicalon CG reinforcement and a 150 nm BN fiber/matrix interface. The irradiation was conducted in the Experimental Breeder Reactor-II at a nominal temperature of 1000°C to doses of either 33 or 43 dpa-SiC. Irradiation caused complete fiber/matrix debonding in the CVI SiC composites due to a dimensional stability mismatch between fiber and matrix, while the PIP SiC composites partially retained their fiber/matrix interface after irradiation. However, the thermal expansion of all the materials tested was found to be primarily dependent on the matrix and independent of either the fiber or the fiber/matrix interface. Further, irradiation had no significant effect on thermal expansion for either the CVI SiC or PIP SiC composites. In general, the thermal expansion of the CVI SiC composites exceeded that of the PIP SiC composites, particularly at elevated temperatures, but the expansion of both matrix types was less than chemical vapor deposited (CVD) β-SiC at all temperatures.

INTRODUCTION

Silicon carbide (SiC) has long been considered an attractive material for use in a fusion reactor environment because of its excellent high-temperature strength and thermal conductivity, dimensional stability during irradiation, and low neutron activation. However, monolithic SiC is not a suitable choice for structural applications due to its brittle nature. In contrast, SiC-fiber-reinforced/SiC-matrix (SiC_f/SiC) composites have recently been shown to exhibit non-catastrophic failure modes analogous to the plastic deformation exhibited by traditional metallic materials [1,2]. As a result, SiC_f/SiC composites are under consideration as candidate structural materials in several fusion reactor concepts. However, several issues

must be addressed before their inclusion in detailed designs: optimization of constituent materials, refinement of fabrication and processing methods, and characterization of the effect of irradiation on material properties. The present study seeks to quantify the effect of irradiation on the linear thermal expansion of several SiC_f/SiC composites fabricated using different constituent materials and processing routes. Six different SiC_f/SiC composite types were characterized by measuring their thermal expansion in the unirradiated and irradiated conditions over the temperature range 300 to 1000 °C. The irradiation was conducted in the Experimental Breeder Reactor II (EBR-II), in an inert gas atmosphere, at a nominal temperature of 1000 °C, to doses of either 33 or 43 dpa-SiC.

EXPERIMENTAL

Materials

Table 1 lists the composites tested in this study; the densities were measured on single unirradiated samples. Two matrices were studied in combination with Nicalon CG reinforcement: chemical vapor infiltrated (CVI) SiC and liquid-phase polymer impregnated precursor (PIP) SiC. The CVI SiC matrix was nominally fully crystalline β-SiC, and the composites had a total fiber volume fraction near 0.40, with approximately 10% porosity distributed predominantly as planar voids between laminae. The CVI SiC composites possessed a triaxial architecture (0°/±86°), but the fiber loading was approximately five times greater in the 90° direction than the 0° direction, resulting in an essentially uniaxial weave. Accordingly, samples were prepared in both the longitudinal (90°) and transverse (0°) orientations.

The PIP SiC matrices were carbon- and oxygen-rich, and at least partially amorphous, due to incomplete pyrolysis of the polymer precursor. The PIP SiC composites were fabricated with an equiaxed woven 0°/90° fiber architecture and a fiber volume fraction of approximately 0.40. These samples contained less porosity than the CVI SiC composites (approximately 5%), but had lower densities due to the lower degree of matrix crystallinity. Three fibers (Nicalon CG, Tyranno, and HPZ) and two interfaces (150 nm PyC and 150 nm BN) were tested in combination with

the PIP SiC matrix. The densities of the Tyranno- and HPZ-reinforced composites were somewhat lower than the Nicalon/PIP SiC composite due to the lower densities of the fiber reinforcement. The fiber architecture, fiber volume fraction, and porosity of these composites were comparable to the Nicalon/PIP SiC sample.

Table 1. Composites included in the study.

Reinforcement	Weave	Interface	Matrix	Density (g/cm^3)	Vendor
Nicalon CG	0°/±86°	150 nm PyC	CVI SiC	2.58	DuPont
Nicalon CG	0°/±90°	150 nm PyC	PIP SiC	2.20	Dow Corning
Nicalon CG	0°/±90°	150 nm BN	PIP SiC	2.21	Dow Corning
Tyranno	0°/±90°	150 nm PyC	PIP SiC	2.10	Dow Corning
HPZ	0°/±90°	150 nm PyC	PIP SiC	2.12	Dow Corning

Test equipment

No specific American Society for Testing and Materials (ASTM) Standard exists that describes thermal expansion testing of ceramic matrix composites using an alumina pushrod dilatometer. However, the test and data reduction procedures described by ASTM Standard E228-85 were generally applicable and were substantially followed for this study [3]. Thermal expansion was measured using a Theta Dilatronic dilatometer. The dilatometer used an alumina pushrod coupled with a linear variable displacement transducer (LVDT) to detect length changes in the test specimen as a function of temperature. The LVDT contact force and voltage response was calibrated before beginning and midway through the test series. Specimen temperature was measured using a Type S (Pt/Pt-10% Rh) thermocouple placed in contact with the center of the test specimen. The measured length change and thermocouple output voltage were recorded in real time on a pen plotter. Plotter-range response calibration for both length change and thermocouple voltage was verified before each test. Tests were conducted at a nominal specimen heating rate of 2°C/min, from room temperature to approximately 1000°C in flowing helium. After reaching 1000°C, the furnace was shut off, and the specimens were allowed to cool to room temperature within the furnace. Specimen length was

measured using a Bausch and Lomb DR-25C optical gauge both before and after thermal-expansion testing. The optical gauge provided an average accuracy of ± 2.2 μm on unirradiated samples and ± 3.8 μm on irradiated samples, with an average precision of ± 0.7 μm on unirradiated samples and ± 1.2 μm on irradiated samples.

Data reduction

The plot produced during each test was digitized using a fine mesh to provide numerical values for measured length change as a function of thermocouple voltage. Thermocouple voltage was converted to temperature using reference tables provided by the National Bureau of Standards for Type S thermocouples [4]. The digitized length change data were fit using an appropriate function, and elongation (ε) was determined using the expression

$$\varepsilon(T) = \frac{L(T) - L_o}{L_o}, \tag{1}$$

where $L(T)$ refers to the measured length of the sample at an elevated temperature T, and L_o is the initial (room temperature) specimen length.

To obtain true elongation data, it was necessary to account for the intrinsic thermal expansion of the measuring system. There are two approaches outlined in ASTM E228-85 for accomplishing this; the simple difference method (ASTM Method B) was used for this study. To account for system thermal expansion, a standard with known thermal expansion was tested. The measured thermal expansion was then subtracted from the known thermal expansion to obtain a correction factor (B)

$$B = \left(\frac{L - L_o}{L_o}\right)_{known} - \left(\frac{L - L_o}{L_o}\right)_{measured}. \tag{2}$$

To test the correction factor, the thermal expansion of a second standard was measured. The correction factor was added to the measured thermal expansion for the second material, and the result was compared to its known thermal expansion.

By performing repeated calibration tests of this type, both the accuracy and precision of the system were determined.

For this study, a sapphire standard was used to generate correction factors that were validated using a platinum standard; the resulting platinum data are shown in Figure 1. The data are compared to the recommended curve for platinum taken from the Thermophysical Properties Research Center (TPRC) database [5]. The data are accurate to within ± 0.05% (absolute) with respect to the TPRC curve, and the scatter associated with the repeated measurements indicates a precision of approximately ± 0.05% (absolute) as well. However, note that the scatter is not random, but generally displays a systematic drift. This reflects a tendency of the dilatometer load-train expansion to vary over a period of time. Ideally, any systematic drift experienced by the dilatometer would be accounted for by a corresponding drift in the correction factors developed from the reference specimen data. To eliminate-length effects (caused by variations in the pushrod temperature gradient), the standard and test specimens should be the same length. The length of the sapphire standard was comparable to the test specimens, but the platinum and sapphire standards differed in length. The drift exhibited by the platinum data in Figure 1 is therefore most likely explained by a length dependence of the correction factors *(B)*. In effect, the drift measured by the sapphire standard was slightly different than that experienced by the platinum standard. Because of the drift in the correction factors, calibration runs were made after every three SiC_f/SiC tests. The correction factors for each SiC_f/SiC specimen were obtained by linearly interpolating between the bracketing calibration runs.

RESULTS AND DISCUSSION

Irradiation dimensional stability

Table 2 presents the irradiation exposure data for the six irradiated specimens. The samples were irradiated for 185 effective full power days (EFPD) in the EBR-II to fluences of either 2.6×10^{22} or 3.4×10^{22} n/cm^2 (E > 0.1 MeV). The higher fluence corresponds to an axial position near the midplane of the reactor core and was

determined from gamma spectroscopy of a Nb-1Zr dosimetry capsule; the lower fluence corresponds to a position midway between the midplane and top of the core and was extrapolated based on the known axial flux profile of the EBR-II. The fluences correspond to doses of 33 and 43 dpa-SiC in the EBR-II neutron spectrum, assuming threshold displacement energies of 25 eV for Si and 31 eV for C.

Table 2. Fluence and dose exposure for irradiated specimens.

Material	Fluence ($\times 10^{22}$ n/cm^2)	Dose (dpa-SiC)
Nicalon/PyC/CVI SiC (longitudinal)	2.6	33
Nicalon/PyC/CVI SiC (transverse)	2.6	33
Nicalon/PyC/PIP SiC	2.6	33
Nicalon/BN/PIP SiC	2.6	33
Tyranno/PyC/PIP SiC	3.4	43
HPZ/PyC/PIP SiC	3.4	43

The nominal temperature of the specimens during the irradiation was designed to be 1000°C when the reactor was operating at full power. After the shutdown from full power at the end of the irradiation, three brief startup/shutdown cycles were conducted; the peak power during each of the three cycles was less than half of full-reactor power. The time associated with these cycles corresponded to approximately 0.4 EFPD (0.1 dpa-SiC) near the reactor midplane. During this interval, the time-averaged temperature of the specimens would have been significantly less than the designed 1000°C. While this brief decrease in temperature should have little to no effect on the mechanical properties of SiC, it could have a noticeable effect on the thermal properties, including thermal expansion.

The principal type of irradiation-induced damage in ceramic materials is the formation of point defects (vacancy/interstitial pairs) resulting from collisions of incident neutrons and subsequent recoil atoms with the crystal lattice [6]. Previous studies have shown that irradiation-induced swelling in β-SiC is principally due to

the lattice distortion introduced by these point defects; i.e., the lattice expansion created by an interstitial is greater than the lattice contraction created by a vacancy [7]. The concentration of irradiation-induced point defects (and its corresponding effect on swelling) has been shown to be a function of irradiation temperature, decreasing linearly from room temperature to 1000°C [8]. Equilibration of the point-defect concentration has been noted at doses as low as 0.2 dpa-SiC at 500°C [9]. Because the defect concentration decreases with increasing irradiation temperature, it is reasonable to expect an equilibration dose approaching 0.1 dpa-SiC above 500°C.

Table 3 presents irradiation-induced length-change data for the composites and constituent fibers tested in this study. The composite and fiber-length change data were obtained on specimens irradiated in the same experiment as the thermal-expansion specimens. The measurements were made on the composite specimens with the DR-25C optical gauge, both before and after irradiation. The fiber-length change data were obtained by cutting individual tows to a specified length before the irradiation and by measuring their post-irradiation length with a traversing microscope on ruled photographs of each fiber tow.

Table 3. Irradiation-induced length-change measurements.

Material	Dose (dpa-SiC)	Composite $\Delta L/L_o$ (%)	Fiber $\Delta L/L_o$ (%)
Nicalon/PyC/CVI SiC (longitudinal)	33	0.290 ± 0.026	- 3.8 ± 0.4
Nicalon/PyC/CVI SiC (longitudinal)	43	0.320 ± 0.006	- 3.8 ± 0.4
Nicalon/PyC/PIP SiC	43	- 4.99 ± 0.065	- 3.8 ± 0.4
Nicalon/BN/PIP SiC	43	- 3.68 ± 0.052	- 3.8 ± 0.4
Tyranno/PyC/PIP SiC	43	- 7.46 ± 0.076	- 5.6 ± 0.3
HPZ/PyC/PIP SiC	43	- 11.9 ± 0.404	- 10.3 ± 0.3

The CVI SiC composites exhibit slight swelling, which is characteristic of highly crystalline β-SiC and corresponds to an apparent irradiation temperature between 600 and 700°C [8]. At temperatures in excess of the apparent irradiation temperature, the vacancy/interstitial pairs diffuse through the lattice and annihilate, which reduces the length of the specimen through the elimination of

the lattice expansion associated with the point defects. Thus, above approximately 600°C, the observed thermal expansion of the CVI SiC composites should be lower than the intrinsic expansion due to the annihilation of the irradiation-induced point defects.

Note from Table 3 that although the CVI SiC matrix swells slightly during irradiation, the Nicalon fiber shrinks by approximately 4% due to densification associated with crystallization. This dimensional stability mismatch between the fiber and matrix results in complete interfacial debonding, as shown in Figure 2a. Compare this appearance to that shown in Figure 2b for the Nicalon/PyC/PIP SiC material, which is typical of all the PIP SiC composites included in this study. The PIP SiC composites appear to have interfacial ligaments connecting the fiber and matrix. Note from Table 3 that the irradiation-induced shrinkage of the PIP SiC composites is consistent with the shrinkage of the constituent fibers. The more amorphous fibers experience greater crystallization during irradiation and hence exhibit greater densification. The shrinkage of the PIP SiC matrix indicated by the data in Table 3 is also likely due to densification caused by crystallization. The shrinkage of both fiber and matrix thus appears to allow partial retention of the fiber/matrix interface.

Figure 3 shows three of the irradiated PIP SiC matrix composites viewed edge-on. Note the visible distortion caused by the severe irradiation-induced shrinkage of these specimens. The distortion is most apparent for the Tyranno/PyC/PIP SiC and HPZ/PyC/PIP SiC composites, which is consistent with the fact that these materials exhibited the greatest shrinkage of all the specimens in the test matrix. However, the distortion did not significantly affect the ability of the samples to seat properly in the dilatometer specimen holder. The data obtained from these specimens are generally consistent with that of the other PIP SiC composites and are therefore considered reasonably reliable despite the observed deformation.

Thermal dimensional stability

Table 4 presents the specimen lengths measured before and after each thermal-expansion test. In general, the unirradiated specimens were more

dimensionally stable during the tests than the irradiated samples, and the unirradiated CVI SiC specimens were more stable than the unirradiated PIP SiC samples. The same cannot be said of the irradiated specimens, however, since both matrix types exhibited similar length changes during the tests. In general, the length changes were negative, suggesting matrix densification. Densification is most likely due to crystallization of amorphous matrix regions in the unirradiated specimens and point-defect annihilation above the apparent irradiation temperature in the irradiated specimens. However, the length change of the irradiated specimens cannot be universally attributed to densification through defect annealing, because two samples exhibited a length increase. Guidance in ASTM E228-85 suggests that if a length change of greater than ± 0.002% is recorded, consideration should be given to re-testing the specimen. Note that every specimen in the test matrix exceeded this value; it was judged unlikely that re-tests would provide any significant improvement.

Table 4. Pre- and post-test lengths for SiC$_f$/SiC thermal-expansion specimens.

Material	Length (cm)		ΔL (cm)	ΔL (%)
	Pre-test	Post-test		
Unirradiated				
Nicalon/PyC/CVI SiC (longitudinal)	3.8133	3.8130	-0.0003	-0.008
Nicalon/PyC/CVI SiC (transverse)	3.8199	3.8194	-0.0005	-0.013
Nicalon/PyC/PIP SiC	3.7584	3.7567	-0.0017	-0.045
Nicalon/BN/PIP SiC	3.8207	3.8189	-0.0018	-0.047
Tyranno/PyC/PIP SiC	3.8194	3.8164	-0.0030	-0.079
HPZ/PyC/PIP SiC	3.8080	3.8070	-0.0010	-0.026
Irradiated				
Nicalon/PyC/CVI SiC (longitudinal)	3.8239	3.8261	+0.0022	+0.058
Nicalon/PyC/CVI SiC (transverse)	3.8296	3.8254	-0.0042	-0.110
Nicalon/PyC/PIP SiC	3.5753	3.5747	-0.0006	-0.017
Nicalon/BN/PIP SiC	3.6738	3.6729	-0.0009	-0.025
Tyranno/PyC/PIP SiC	3.5537	3.5579	+0.0042	+0.118
HPZ/PyC/PIP SiC	3.3299	3.3253	-0.0046	-0.138

Thermal expansion

Figures 4 and 5 present the combined thermal-expansion data for all the unirradiated and irradiated SiC_f/SiC composites, respectively. Manufacturer data for unirradiated monolithic chemical vapor deposited (CVD) β-SiC are included in Figure 4 for reference [10].

CVI SiC matrix composites

Thermal-expansion data for both the unirradiated and irradiated Nicalon/PyC/CVI SiC composites are shown in Figure 6 for both longitudinal (90°) and transverse (0°) specimen orientations. Note the difference in thermal expansion between the unirradiated longitudinal and transverse specimens and the similarity between the two irradiated samples. Note also that the unirradiated transverse specimen exhibits behavior similar to both irradiated composites. Because the fibers are completely debonded from the matrix after irradiation, as shown in Figure 2a, the post-irradiation thermal expansion should be solely dependent on the behavior of the matrix. Therefore, the difference exhibited between the unirradiated longitudinal specimen and the two irradiated specimens may be due to the presence of the fibers. Although the fibers may contribute somewhat to the thermal expansion in the unirradiated longitudinal specimen, it appears that they have an insignificant effect in the unirradiated transverse specimen, based on the similarity between it and the matrix-dominated irradiated specimens.

A further conclusion to be drawn from the similarity between the unirradiated transverse specimen and both irradiated specimens is that irradiation to 33 dpa-SiC has little effect on thermal expansion of the CVI SiC matrix. Although the bulk of the irradiation was conducted at 1000°C, the apparent irradiation temperature based on the point-defect concentration in the samples was between 600 and 700°C. This can be seen from the data in Figure 6 by the knee in the thermal-expansion curve of the irradiated samples at approximately 700°C. Annealing of point defects above this temperature caused the rate of thermal expansion to decrease, yielding a decrease in the slope of the thermal-expansion curve. However, this effect is small

and within the limits of the experimental uncertainty. Thus, the only significant effect of irradiation on the CVI SiC composites is interfacial debonding, which eliminates any influence the fibers may have on the thermal expansion in the longitudinal orientation.

PIP SiC matrix composites

Figures 7 through 10 present comparisons of unirradiated and irradiated data for Nicalon/PyC/PIP SiC, Nicalon/BN/PIP SiC, Tyranno/PyC/PIP SiC, and HPZ/PyC/PIP SiC composites, respectively. Note from Figures 4 and 5 that the thermal expansion of the four PIP SiC composites is the same, within experimental uncertainty, in both the unirradiated and irradiated condition, in spite of significant differences in fiber and interface materials. Note also the consistent difference in thermal expansion between the Nicalon/PyC/CVI SiC and Nicalon/PyC/PIP SiC composites. These observations provide reasonable evidence to conclude that the thermal expansion of the PIP SiC materials is dominated by the matrix. The partial retention of the fiber/matrix interface in the PIP SiC composites after irradiation does not significantly influence thermal expansion.

No consistent trends are evident in the data to suggest that fast neutron irradiation from 33 to 43 dpa-SiC has a noticeable effect on thermal expansion of PIP SiC matrix composites. Note from Figures 7 through 10 that the thermal expansion of the unirradiated and irradiated PIP SiC composites is the same within the uncertainty of the measurement technique. Note also that the thermal expansion curves for three of the irradiated PIP SiC composites exhibit an increase in slope above the apparent irradiation temperature of 600 to 700°C. This behavior is contrary to that expected from point-defect annealing, and its cause is unclear.

The CVI SiC composites exhibit generally higher thermal expansion than the PIP SiC composites, particularly above 600°C for the unirradiated materials and 200°C for the irradiated materials. Because the thermal expansion of these composites appears to be independent of the fiber reinforcement and interface in the irradiated condition, the difference between CVI SiC and PIP SiC composites is most likely due to the inherent differences in thermal expansion of the two matrix

materials. The fact that a discernible difference exists between the two matrix types is not surprising, considering their dramatically different processing routes and resultant microstructures.

Note that the thermal expansion exhibited by both the CVI SiC matrix and PIP SiC matrix materials is less than that for CVD β-SiC, as illustrated in Figure 4. Because the fibers do not appear to contribute to the thermal expansion of the composites, the differences between CVD β-SiC and CVI SiC or PIP SiC are most likely due to inherent differences in composition and/or microstructure. Intuitively, one would expect the CVI SiC material to behave more like CVD β-SiC, due to its more crystalline microstructure and stoichiometric composition. This assumption appears to be confirmed by the data in Figure 4.

CONCLUSIONS

Fast-neutron irradiation to 33 dpa-SiC at 1000°C causes complete fiber/matrix interface debonding in CVI SiC matrix composites. The thermal expansion of the irradiated CVI SiC composites is therefore dominated by the matrix material. This is evident from the fact that the thermal expansion of the essentially uniaxial CVI SiC composites is the same (within the precision of the measurement technique) in both the longitudinal and transverse orientations after irradiation. The thermal expansion in the unirradiated condition in the transverse orientation is comparable to that for the irradiated condition, indicating that expansion in this orientation in the unirradiated condition is also dominated by the matrix. The thermal expansion of the unirradiated longitudinal specimen is somewhat different than either the unirradiated transverse specimen or the irradiated specimens. This suggests some possible influence of the fibers on thermal expansion in the longitudinal orientation in the unirradiated condition. The effect of irradiation on thermal expansion of the CVI SiC composites is limited to eliminating any apparent contribution of the fibers to expansion in the longitudinal orientation through interface debonding.

The thermal expansion of PIP SiC composites with Nicalon CG, Tyranno, and HPZ reinforcement, as well as 150 nm PyC and 150 nm BN fiber/matrix interfaces, is

the same to within experimental uncertainty in both the unirradiated and irradiated conditions. Thus, the PIP SiC matrix appears to dominate the thermal-expansion behavior of these composites. Also, no consistent trends are evident in the data to suggest that fast-neutron irradiation from 33 to 43 dpa-SiC at 1000°C has a significant effect on thermal expansion of PIP SiC matrix composites. Although the PIP SiC composites exhibit partial retention of the fiber/matrix interface after irradiation, this has no apparent effect on the composite thermal expansion due to the negligible contribution of the fibers to expansion.

In general, the thermal expansion of the CVI SiC composites is slightly higher than for the PIP SiC composites. This effect is particularly noticeable at temperatures above 600°C for the unirradiated specimens and above 200°C for the irradiated specimens. Because thermal expansion appears to be dominated by the matrix materials, these differences are assumed to arise from the inherent differences in the matrices. The thermal expansion of both matrix types is less than CVD β-SiC at all temperatures below 1000°C. This is interpreted as being due to inherent differences in composition and/or microstructure between CVD β-SiC and the CVI SiC and PIP SiC matrices.

From the point of view of thermal expansion, the CVI SiC and PIP SiC composites performed equally well under irradiation to 33 and 43 dpa-SiC, respectively. The thermal expansion of the materials tested is not dramatically different than CVD β-SiC, and should be relatively simple to predict due to the lack of dependence on the fiber reinforcement. However, if a dimensionally stable fiber and/or interface is used that does not debond from the matrix during irradiation, the fibers and interface may then influence thermal expansion. Fusion reactor component design is also simplified by the fact that the thermal expansion of these materials is unaffected by irradiation to 33 or 43 dpa-SiC, although irradiation-induced swelling considerations must still be taken into account.

References

1. Hollenberg, G.W., C.H. Henager, G.E. Youngblood, D.J. Trimble, S.A. Simonsen, G.A. Newsome, and E. Lewis. 1995. "The Effect of Irradiation on

the Stability and Properties of Monolithic Silicon Carbide and SiC_f/SiC Composites up to 25 dpa," *J. Nucl. Mat.*, 219:70-86.

2. Woodford, D.A., D.R. Van Steele, J.A. Brehm, L.A. Timms and J.E. Palko. 1993. "Testing the Tensile Properties of Ceramic-Matrix Composites," *JOM*, 45(5):57-63.

3. American Society for Testing and Materials. 1989. "Standard Test Method for Linear Thermal Expansion of Solid Materials with a Vitreous Silica Dilatometer," *ASTM E228-85*. Philadelphia, PA: American Society for Testing and Materials.

4. Powell, R.L., W.J. Hall, C.H. Hyink, L.L. Sparks, G.W. Burns, M.G. Scroger and H.H. Plumb. 1974. "Thermocouple Reference Tables Based on the IPTS-68," *NBS Monograph 125*. Washington, DC: National Bureau of Standards.

5. Touloukian, Y.S., R.K. Kirby, R.E. Taylor, and T.Y.R. Lee. 1977. *Thermal Expansion of Metallic Elements and Alloys*. New York, NY: Plenum Press.

6. Olander, D.R. 1976. "Fundamental Aspects of Nuclear Reactor Fuel Elements," *TID-26711-P1*, Washington, DC: Energy Research and Development Administration.

7. Price, R.J. 1973. "Thermal Conductivity of Neutron-Irradiated Pyrolytic β-Silicon Carbide," *J. Nucl. Mat..*, 46:268-272.

8. Price, R.J. 1977. "Properties of Silicon Carbide for Nuclear Fuel Particle Coatings," *Nucl. Tech.*, 35:320-336.

9. Yano, T., K. Sasaki, T. Maruyama, T. Iseki, M. Ito, and S. Onose. 1991. "A Step-Heating Dilatometry Method to Measure the Change in Length Due to Annealing of a SiC Temperature Monitor," *Nucl. Tech.*, 93:412-415.

10. Morton Advanced Materials. 1994. "CVD Silicon Carbide," *Technical Bulletin 107*. Woburn, MA: Morton International.

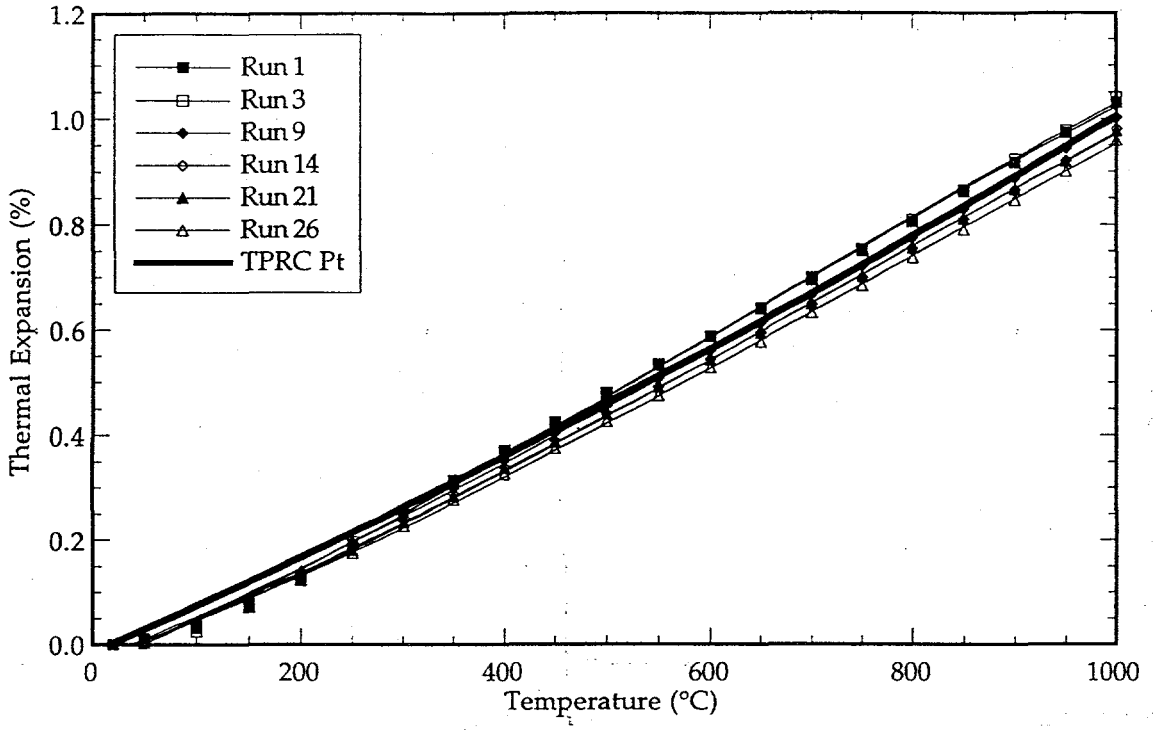

Figure 1. Linear thermal expansion of platinum standard calculated using correction factors obtained from sapphire standard.

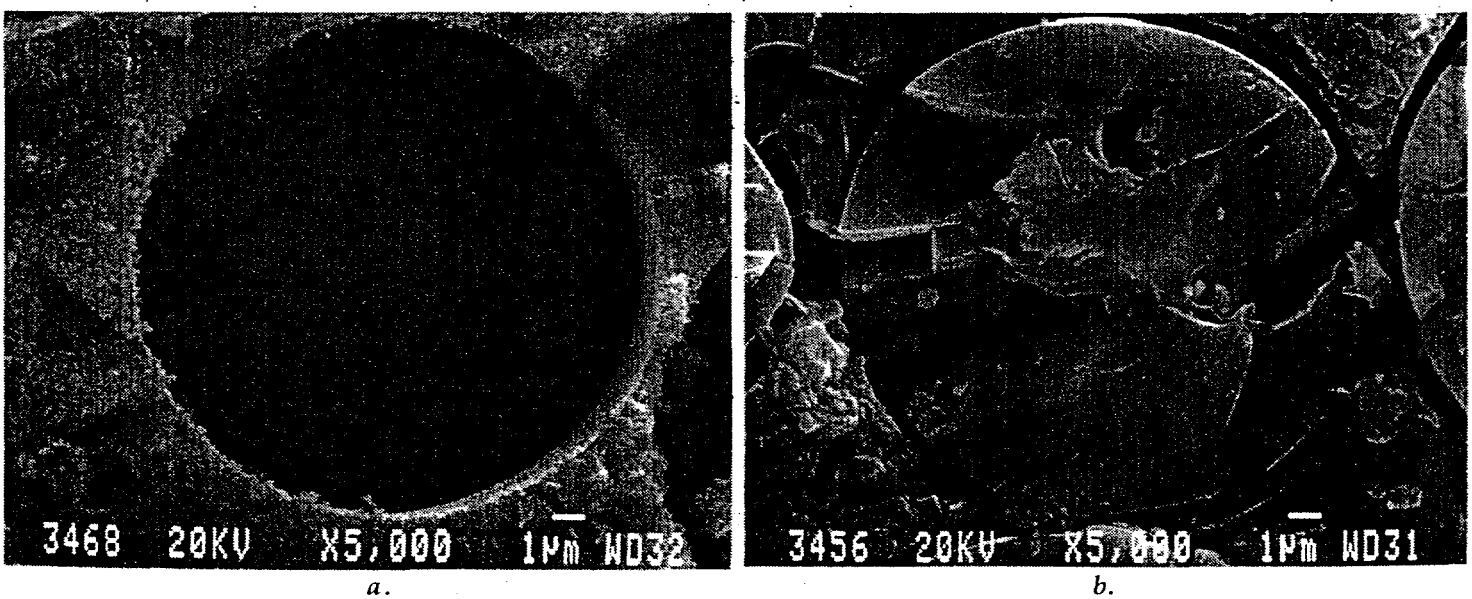

a. *b.*

Figure 2. Post-irradiation views of single fibers in a) Nicalon/150-nm PyC/CVI SiC and b) Nicalon/150-nm PyC/PIP SiC showing the condition of the fiber/matrix interface.

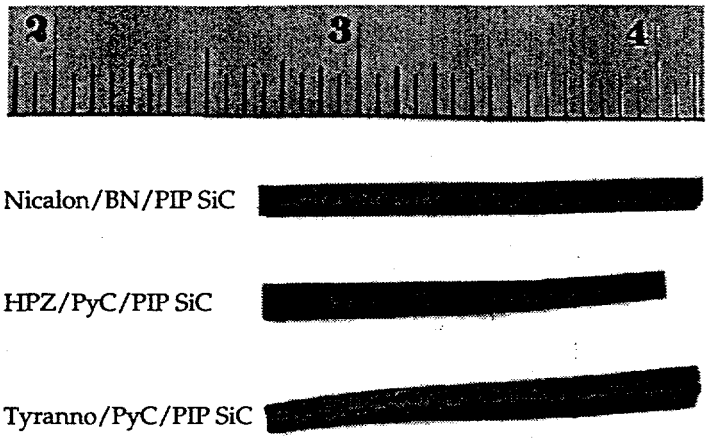

Figure 3. Edge view of irradiated PIP SiC composite thermal-expansion specimens showing visible distortion due to irradiation-induced shrinkage.

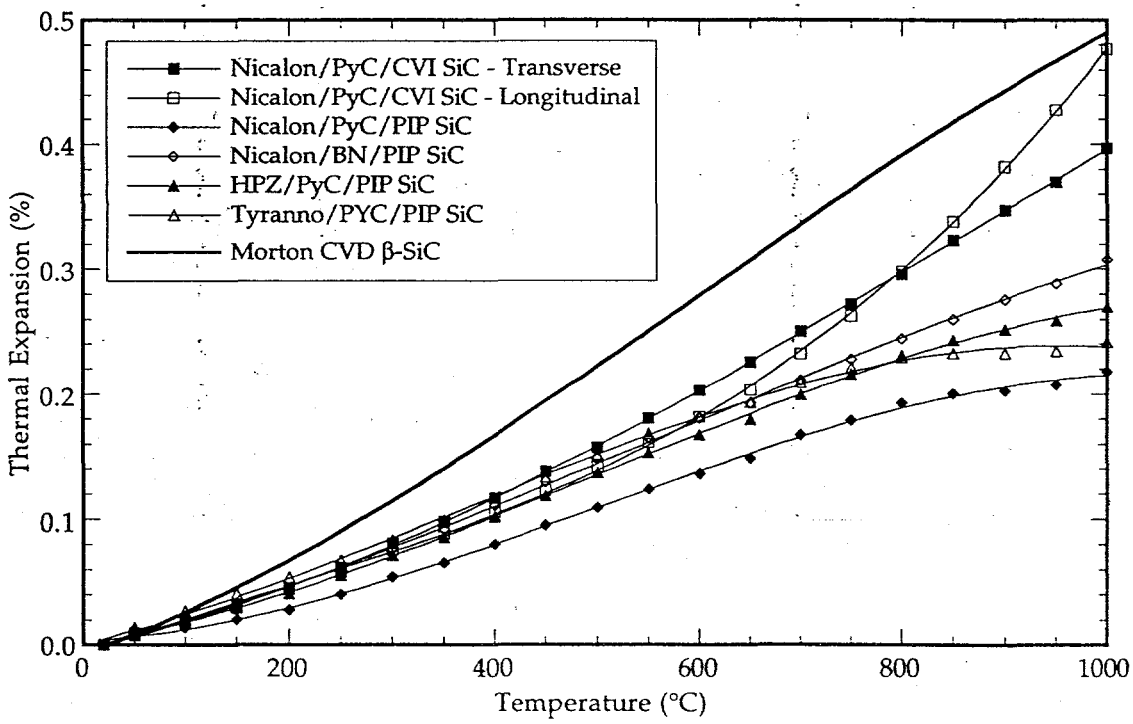

Figure 4. Linear thermal expansion of unirradiated SiC_f/SiC composites.

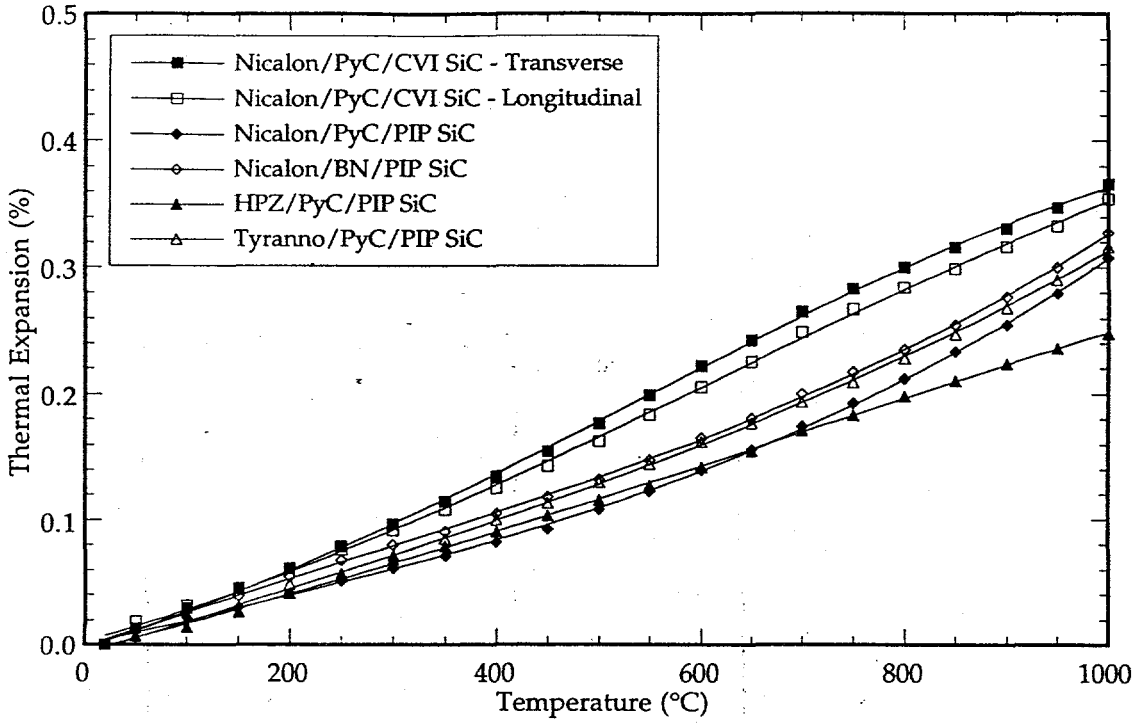

Figure 5. Linear thermal expansion of irradiated SiC_f/SiC composites.

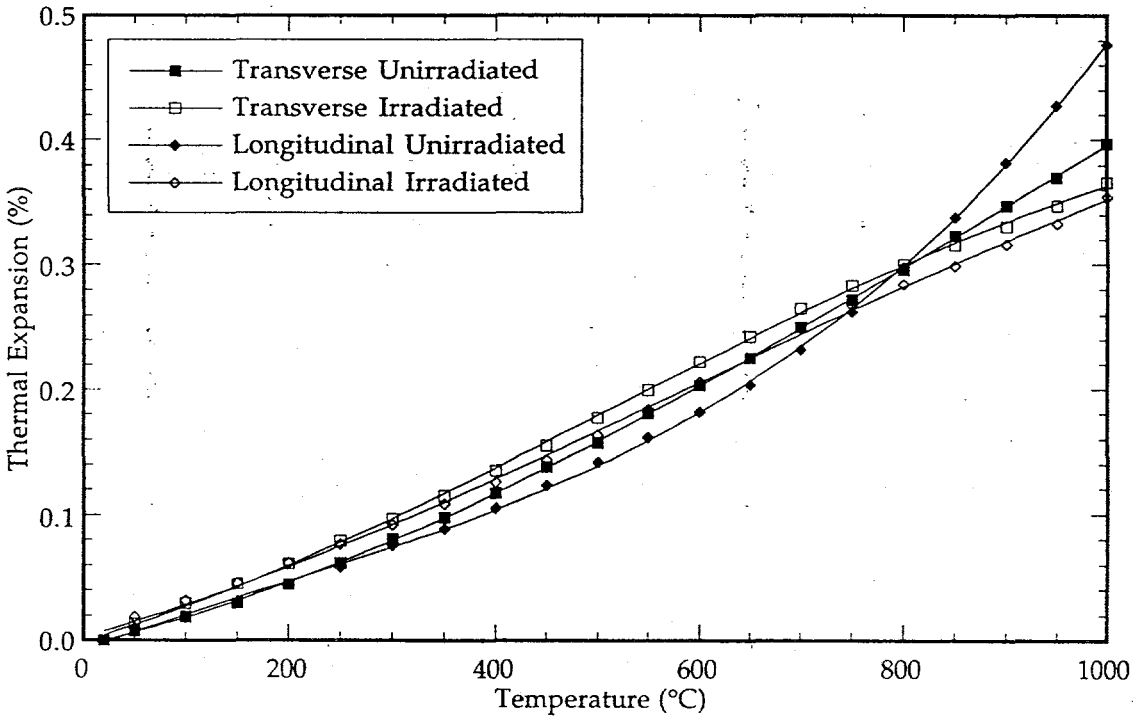

Figure 6. Linear thermal expansion of unirradiated and irradiated Nicalon/150-nm PyC/CVI SiC composites.

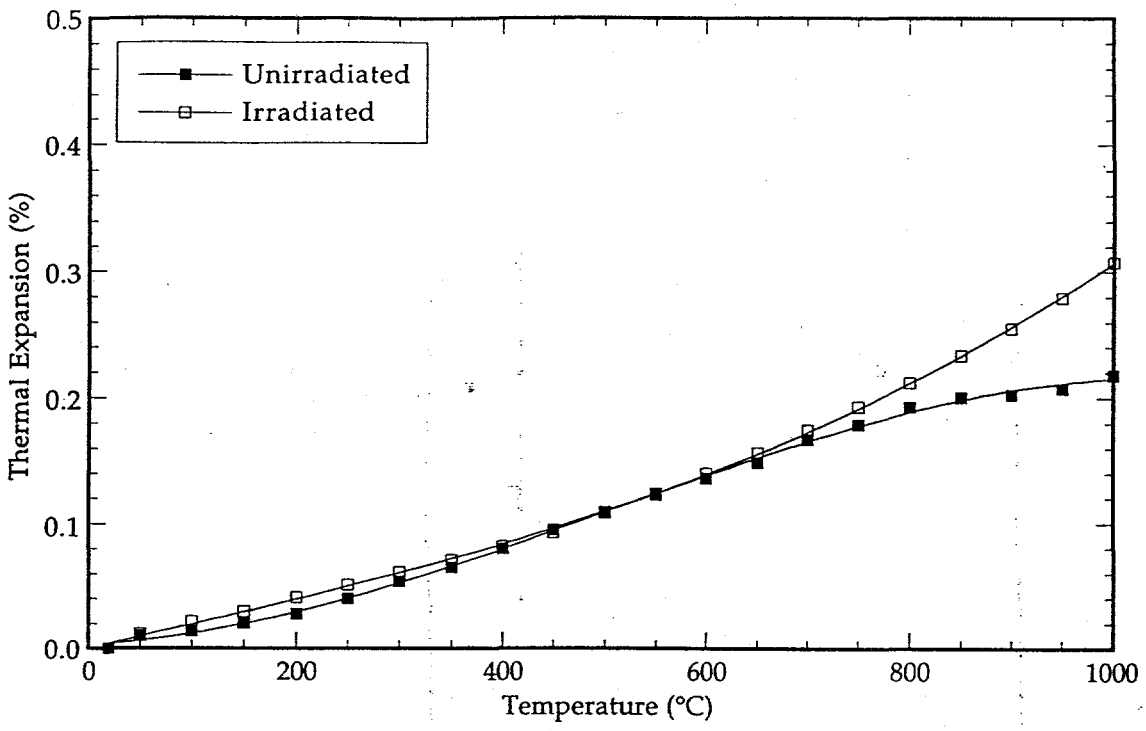

Figure 7. Linear thermal expansion of unirradiated and irradiated Nicalon/150-nm PyC/PIP SiC composites.

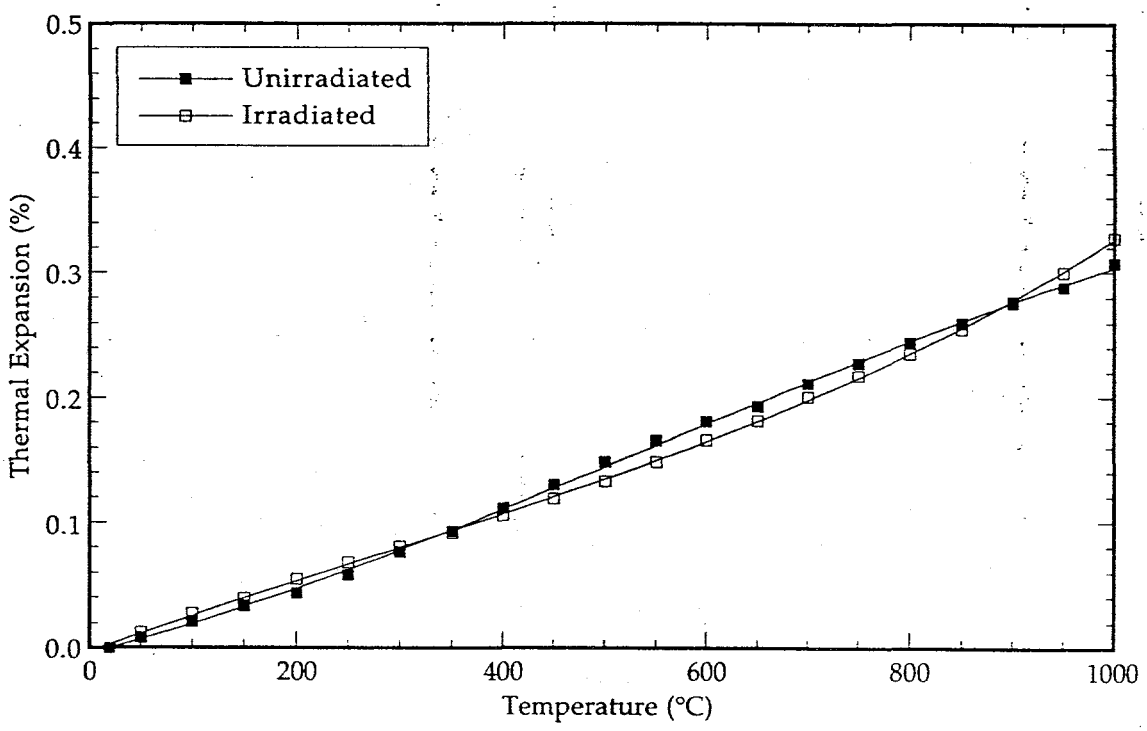

Figure 8. Linear thermal expansion of unirradiated and irradiated Nicalon/150-nm BN/PIP SiC composites.

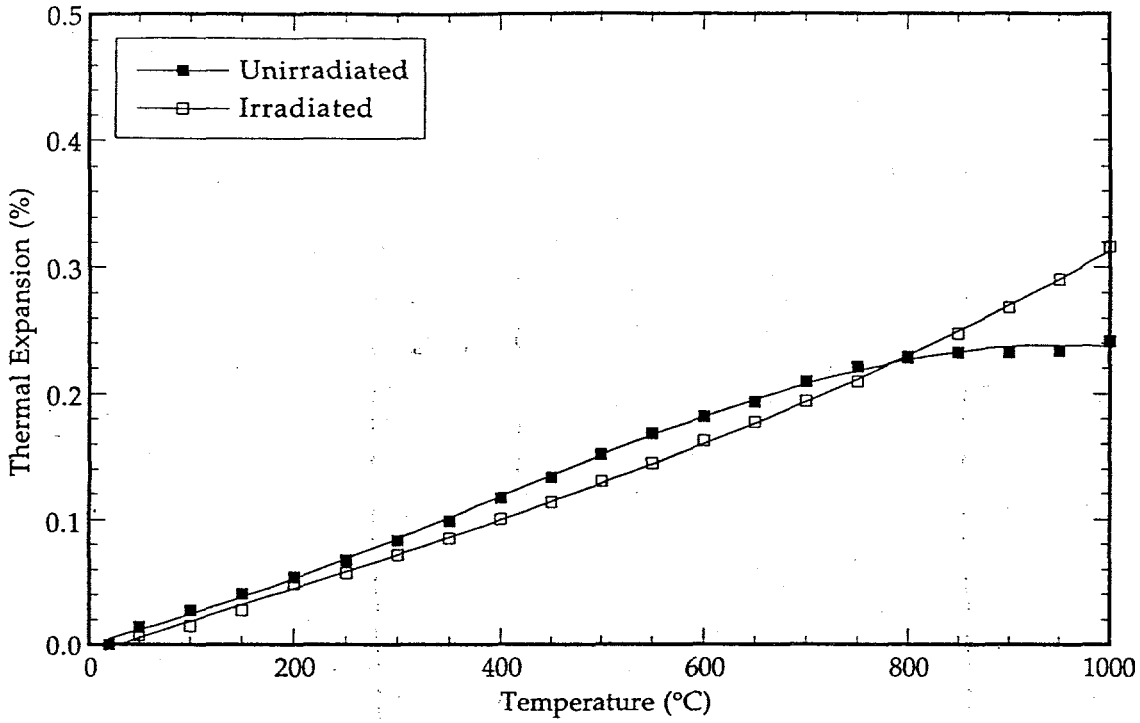

Figure 9. Linear thermal expansion of unirradiated and irradiated Tyranno/150-nm PyC/PIP SiC composites.

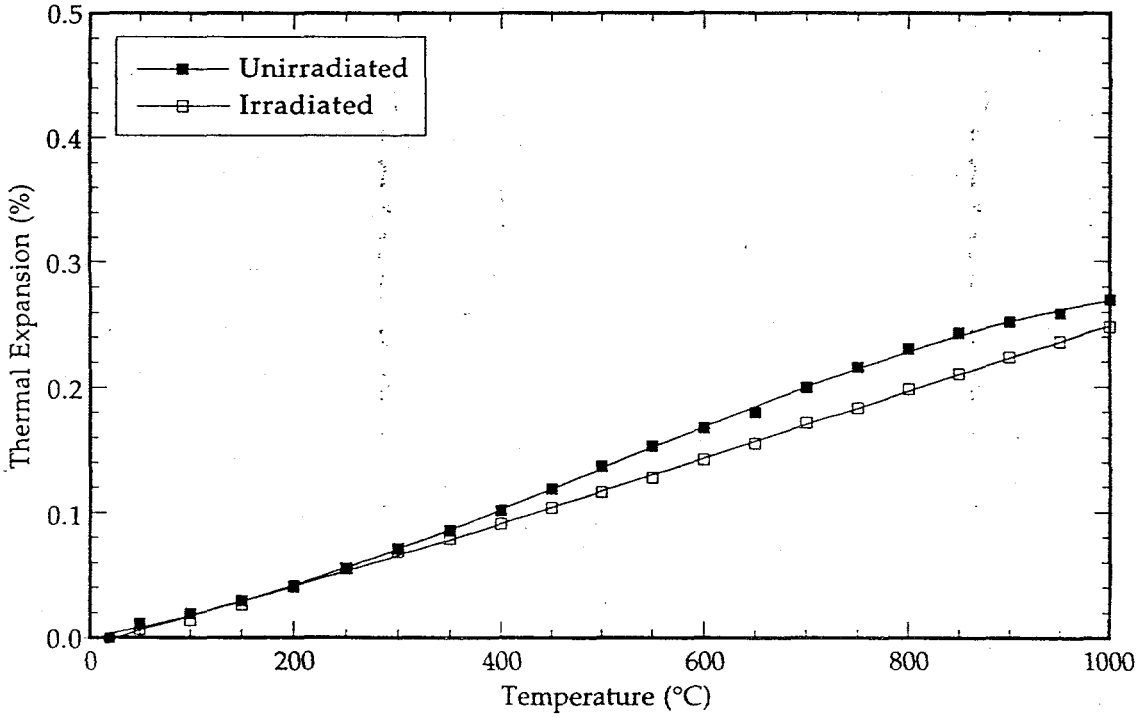

Figure 10. Linear thermal expansion of unirradiated and irradiated HPZ/150-nm PyC/PIP SiC composites.